Carrier dynamics in Si nanocrystals in an SiO_2 matrix investigated by transient light absorption

W. D. A. M. de Boer, E. M. L. D. de Jong,* D. Timmerman, and T. Gregorkiewicz
Van der Waals-Zeeman Institute, University of Amsterdam, Amsterdam, The Netherlands

H. Zhang and W. J. Buma
Van 't Hoff Institute for Molecular Sciences, University of Amsterdam, Amsterdam, The Netherlands

A. N. Poddubny, A. A. Prokofiev, and I. N. Yassievich
Ioffe Physical-Technical Institute, Russian Academy of Sciences Polytechnicheskaya 26, 194021 Saint-Petersburg, Russia
(Received 6 June 2013; revised manuscript received 23 July 2013; published 8 October 2013)

We report on investigations of optical carrier generation in silicon nanocrystals embedded in an SiO_2 matrix. Carrier relaxation and recombination processes are monitored by means of time-resolved induced absorption, using a conventional femtosecond pump-probe setup for samples containing different average sizes of nanocrystals (d_{NC} = 2.5–5.5 nm). The electron-hole pairs generated by the pump pulse are probed by a second pulse over a broad spectral range (E_{probe} = 0.95–1.35 or 1.6–3.25 eV), by which information on excited states is obtained. Under the same excitation conditions, we observe that the induced absorption intensity in the near-infrared range is a factor of ∼10 higher than in the visible range. To account for these observations, we model the spectral dependence of the induced absorption signal using an empirical $sp^3d^5s^*$ tight-binding technique, by which the spectrum can be well reproduced up to a certain threshold. For probe photon energies above this threshold (dependent on nanocrystal size), the induced absorption signal is found to feature a long-standing component, whereas the induced absorption signal for probe photon energies below this value vanishes within 0.5 ns. We explain this by self-trapping of excitons on surface-related states.

DOI: 10.1103/PhysRevB.88.155304 PACS number(s): 78.67.Bf, 78.67.Hc, 71.35.Cc, 73.22.Dj

I. INTRODUCTION

The most successful way to manipulate the energy structure of silicon (Si) has been achieved via quantum confinement in nanostructures. Due to the possibility to induce changes in the energy structure by space quantization, semiconductor nanocrystals (NCs) have emerged as ideal candidates for multiple applications. Si NCs have been intensively studied and a considerable amount of information on ensembles and on individual NCs has been collected. In particular, it has been established that the excitonic emission from Si NCs has two characteristic features: for smaller grains, the photoluminescence (PL) spectrum shifts to the blue and its intensity increases. These observations reflect the opening up of the (indirect) band gap and the enhancement of the radiative recombination rate of electron-hole pairs, as momentum conservation is gradually relaxed for smaller grains due to the Heisenberg principle (while the transition itself remains indirect in momentum space).[1] Further, a possible participation of an oxygen-related interface state in photon emission has been suggested, leading to stabilization of the PL wavelength for Si NCs smaller than ∼2.5 nm in diameter.[2]

Details of the mechanisms responsible for light emission can be clarified by investigations of the carrier dynamics at short times after photoexcitation. Fast initial carrier relaxation can be studied by femtosecond (fs) transient induced absorption (IA). Ultrafast carrier dynamics in Si NCs, either obtained by fs IA or PL up-conversion, always exhibits a multiexponential decay as a consequence of various carrier relaxation pathways. These components have in the past been assigned to carrier relaxation processes such as trapping at surface states,[3] carrier cooling via carrier-carrier scattering, Auger transfer between (hot) electrons and holes,[4] phonon-assisted cooling,[5] or radiative decay via a phononless recombination channel.[3,6–10] For oxygen-passivated Si NCs, it has been shown that carrier cooling can be slowed down by three orders of magnitude in comparison to bulk Si,[10] thus effectively enhancing the role of trapping processes. The interplay between electronic surface states and conduction-band states for surface-modified Si NCs may be quantitatively elucidated by direct monitoring photoexcited carrier dynamics with fs spectroscopy. Up to now, a direct correlation between results obtained with IA and PL spectroscopy is still missing.

In this study, we report on ultrafast IA dynamics detected for a spectrally broad range (E_{det} = 0.95–3.25 eV) in Si NCs embedded in an oxygen-rich environment. These NCs are characterized by the typical red emission, which blue-shifts for smaller NC sizes. We correlate experimentally observed IA spectra with simulations within an $sp^3d^5s^*$ tight-binding model, by which theoretical values for the IA cross section are obtained. For the near-infrared (NIR) range, values of the order of $\sim 10^{-17}$ cm^2 were found, and are one order of magnitude smaller for the visible range. Compared to the linear absorption, the IA cross section in the NIR range is found to be at least one order of magnitude higher, while in the visible range, the opposite is observed. In addition, a long-standing absorption component is observed for detection photon energies exceeding a certain threshold, whereas for the low photon energy range, the IA signal vanishes within 0.5 ns. The latter effect has in the past been assigned to carrier trapping and formation of self-trapped excitons (STEs) at the surface of the NC.[11]

This paper follows on our recent preliminary paper[11] where highlights of the project have been given. Building on that we now (i) present IA results, as obtained by both experiment

and theory, for the full spectral range, (ii) show IA spectra for a broad range of excitation energies, (iii) provide the full account of theoretical modeling of the IA cross section, (iv) elaborate on the IA dynamics, and (v) extend the self-trapped exciton model.

II. EXPERIMENTAL DETAILS

The study has been performed on Si NCs embedded in an SiO_2 matrix, which were prepared by a radio-frequency co-sputtering method. The deposited films are about 1 μm thick and are annealed in a N_2 gas atmosphere for 30 min at temperatures ranging from 1000 °C to 1200 °C. By tuning the excess of Si and the annealing temperature, samples with typical average NC sizes ranging from $d_{NC} = 2.5$–5.5 nm were obtained with a relatively high NC density of the order of $n_{NC} \approx 10^{18}$ cm^{-3} and a relatively narrow log-normal size distribution with $\sigma \approx 19\%$, which was similar for all samples used in the current study. The formation of spherelike Si NCs is confirmed by high-resolution transmission electron microscopy (HRTEM) images (see Ref. 12) and d_{NC} is estimated from the steady-state PL measurements and using Fig. 3 from Ref. 12. For IA experiments, a pump-probe setup was employed, consisting of an optical parametric amplifier pumped by a chirped-pulse amplified Ti:sapphire laser with a repetition rate of $f = 1$ kHz (resolution ~200 fs). The pump and probe pulses were directed through different optical paths, where in the latter case a (folded) mechanical delay line has been implemented to tune the mutual timing of both pulses (with a maximum of $\Delta t \approx 3.5$ ns). Prior to impinging onto the sample, the probe pulse is spectrally converted into a white light ($E_{probe} = 0.95$–1.35 eV) or NIR continuum ($E_{probe} = 1.6$–3.25 eV) with the aid of a water cell or a CaF_2 film so that wavelength-dependent features can be resolved. As a consequence of strong (anti-)Stokes broadening and group-velocity dispersion, the pulse is stretched both spectrally and temporally, resulting in a 200-fs broad pulse. This effect leads to a photon-energy-dependent arrival time of the probe at the sample, referred to as "chirp." For the samples used in this study, the latter effect does not show significant contribution and the width of the pulse is in the $\Delta t \approx 240$–360 fs range, dependent on the detection photon energy. The IA signal was detected with a multichannel charge-coupled device (CCD) camera, and registered as $I_{IA} = (I_{total}\text{-}I_{lin\ abs})/I_{lin\ abs}$. Here, I_{IA} is the IA signal, I_{total} the combined linear and IA of the probe pulse, and $I_{lin\ abs}$ the linear absorption, which is subtracted to extract the contribution of the excited-state absorption. The IA signal is normalized to the linear absorption of the probe. In this way, a percentage of the IA is obtained and longer-term fluctuations of the laser power (between I_{IA} signals at different detection energies E_{det}) are eliminated. Moreover, the recorded IA spectra can thus be reliably assigned to NC-intrinsic characteristics. All experiments were performed at room temperature and the IA spectra are corrected for the chirp.

III. THEORETICAL MODELING OF IA CROSS SECTION

The major contribution to IA comes from free carriers. In bulk Si, the intraband absorption of light is a phonon-assisted process, described by the Drude model. In Si NCs, phononless processes become possible. Therefore, in order to obtain information about the IA cross section, the free-carrier absorption spectra as a function of excitation photon energies have been modeled for different NC diameters using two different theoretical approaches: the Drude model for phonon-assisted transitions and a tight-binding model for phononless ones. Both of these processes contribute to the total IA cross section.

A. Drude model

Conventionally for bulk materials, the (photon-energy-dependent) IA cross section can be obtained using the Drude model.[13,14] The development of the free-carrier (or IA) signal for a given probe photon energy E_{probe} for different time delays between pump and probe pulses can be described with the relation $I_{IA}(E_{probe},t) \propto \sigma_{IA}(E_{probe}) \times n_{exc}(t)$, where σ_{IA} is the free-carrier-absorption cross section and n_{exc} the concentration of free electron-hole pairs (or excitons) as a function of time; n_{exc} decreases in time due to, e.g., recombination and trapping of the generated carriers. The free-carrier-absorption cross section σ_{IA} is the sum of the free-carrier absorption of electrons and holes: $\sigma_{IA} = \sigma_e + \sigma_h$. The absorption by free carriers in case of bulk Si is accompanied by scattering (with acoustic phonons or at impurity centers) to compensate for the momentum mismatch between the initial and final states. Within the Drude model, in a simple parabolic energy dispersion, the free-carrier-absorption cross section $\sigma_{e,h}$ (for either electron or holes) is given by the following relation:[13]

$$\sigma_{e,h}(E_{probe}) = \frac{e^2h^2}{4\pi^2\varepsilon_0 c(E_{probe})^2 m^* n}\frac{1}{\tau_s}, \qquad (1)$$

where e is the electron charge, h is Planck's constant, c and ε_0 are the velocity of light in vacuum and the permittivity of the free space, respectively, n is the refractive index, m^* is the carrier effective mass, and τ_s is the average scattering time of charge carriers. The mean scattering time for carriers in a bulk semiconductor τ_s^{bulk} can be estimated from their mobility μ as $\tau_s^{bulk} = \mu m^*/e$. In the case of Si, we take for m^* the conductivity effective mass value, which for electrons is $m_e^* = 0.26m_0$ and for holes $m_h^* = 0.5m_0$.[15] This then leads to a scattering time $\tau_s^{bulk} \approx 4\times\ 10^{-13}$ s for both electrons and holes at room temperature. The $(E_{probe})^{-2}$ dependence of the IA cross section results in a gradual decrease of the IA cross section as a function of photon energy, with values of the order of ~10^{-18}–10^{-16} cm^2 at room temperature for the investigated probe photon energy range [see light and dark green lines in Fig. 1(a) for electrons and holes, respectively]. In the past, the Drude model has been applied to find free-carrier cross sections for excitons confined in Si NCs, and it has been concluded that the experimentally observed dependence could be well described with Eq. (1).[13] The values for the cross section in case of NCs were increased by a factor ~10 compared to bulk Si which was considered to be a consequence of the decreased mean-free path limited by the diameter of the NC. This is demonstrated in Fig. 1(a) for NCs with an average NC diameter of $d_{NC} = 5$ nm by the magenta lines (light: electrons, dark: holes). However, the discretization of energy levels in NCs is not considered within this theoretical

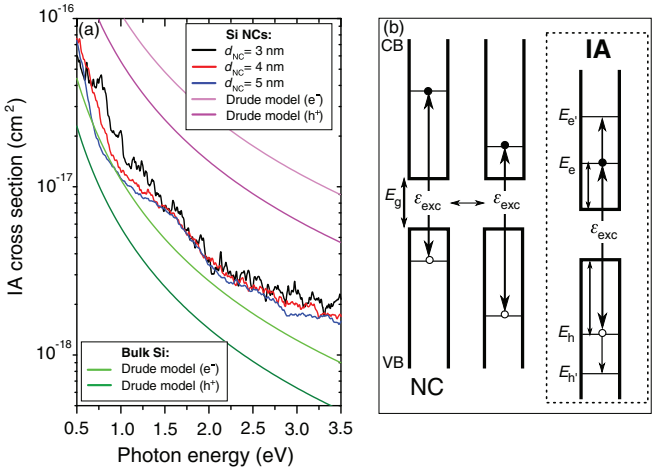

FIG. 1. (Color online) Theoretical spectral dependence of IA. (a) Drude model with $(E_{\text{probe}})^{-2}$ dependence, as described by Eq. (1), for electrons (light green) and holes (dark green) in bulk Si and in Si NCs (electrons: light magenta; holes: dark magenta) for the photon energy range of $E_{\text{probe}} = 0.5$–3.5 eV plotted together with simulations obtained within the tight-binding approximation for NC sizes of $d_{\text{NC}} = 3$ nm (black), $d_{\text{NC}} = 4$ nm (red), and $d_{\text{NC}} = 5$ nm (blue). (b) Schematic illustration of the redistribution of exciton energy $\mathcal{E}_{\text{exc}}$ by Auger energy transfer between carriers in Si NCs with band-gap energy E_g. CB and VB indicate conduction and valence bands, respectively. The right side of the panel shows absorption of photons with energy $\mathcal{E}_{\text{exc}}$ by "free" electrons and holes in initial states E_e and E_h to final states $E_{e'}$ and $E_{h'}$, respectively.

approach. Therefore, it is necessary to apply a new approach taking into account the discretization of energy levels under quantum confinement. The absorption of free carriers has been modeled previously by applying a pseudopotential technique for low-photon energies in a narrow region, and with the confined carriers in equilibrium thermal distribution.[16] In the next section, we present modeling of the spectral behavior of the IA cross section for conditions corresponding to the current experiment.

B. Tight-binding technique

An empirical $sp^3d^5s^*$ tight-binding technique is applied, including spin-orbit interaction,[17] as has been done in the past in similar systems but over a more limited spectral range.[16] The states of confined carriers were calculated for hydrogen-passivated Si clusters;[18,19] hydrogen-bonding parameters have been taken from Ref. 19. Generally, the initial distribution of carriers after photon absorption mainly consists of "hot" electrons and "cold" holes.[20] Subsequently, due to very high rates of Auger-type energy exchange between the carriers inside the NC (with characteristic times $\tau \lesssim 10^{-13}$ s), energy is redistributed between holes and electrons,[20] such that hot carriers are homogeneously dispersed through all energy levels. This is schematically illustrated in the left side of Fig. 1(b), where a "hot" exciton with energy $\mathcal{E}_{\text{exc}}$ is shown with the electron and hole populating different levels in the conduction and valence bands, respectively. Therefore, distribution of carriers in NCs needs to be described by a joint two-particle distribution function. The (re)distributed "hot free excitons" have energy $\mathcal{E}_{\text{exc}} = E_g + |E_e| + |E_h|$, with E_g the NC band gap and E_e and E_h electron and hole energies in conduction and valence bands, respectively.

The IA cross section σ_{IA} (averaged over the ensemble of NCs) was modeled as a function of the probe photon energy $h\nu$ for various exciton energies $\mathcal{E}_{\text{exc}}$ at the moment of maximum overlap between pump and probe pulses:

$$\langle \sigma_{\text{IA}}(E_{\text{probe}}) \rangle = \sum_{e,e',h,h'} f_{e,h}(\mathcal{E}_{\text{exc}}) \hbar\omega_0 [\tilde{\sigma}_{ee'} S_\delta(E_{e'} - E_e - E_{\text{probe}}) + \tilde{\sigma}_{hh'} S_\delta(E_h - E_{h'} - E_{\text{probe}})]. \quad (2)$$

The equation considers intraband transitions between different states, where summation over all electron (e,e') and hole states (h,h') is performed. The corresponding energies of the initial and the final states are E_e and $E_{e'}$ for electrons, and E_h and $E_{h'}$ for holes, respectively; a schematic illustration is shown in the right side of Fig. 1(b) in the dashed rectangle. The energy of the final electron and hole states $E_{e'}$ and $E_{h'}$ is determined by the probe photon energy $E_{\text{probe}} = h\nu$. The distribution function $f_{e,h}(\mathcal{E}_{\text{exc}})$ gives the probability of an exciton with the electron in state e and the hole in state h for which the total energy (including E_g) adds up to $\mathcal{E}_{\text{exc}}$. The function $f_{e,h}(\mathcal{E}_{\text{exc}})$ was chosen as a Gaussian distribution $f_{e,h}(\mathcal{E}_{\text{exc}}) = \mathcal{N} e^{-(E_e+E_g-E_h-\mathcal{E}_{\text{exc}})^2/\Delta^2}$, with $\Delta = 100$ meV, which accounts for the spread in band-gap energy due to the NC size distribution in these samples. The quantity $\mathcal{N}$ is a normalization factor found from the condition $\sum_{e,h} f_{e,h}(\mathcal{E}_{\text{exc}}) = 1$, corresponding to one exciton per NC. Further, the intraband absorption cross sections $\tilde{\sigma}_{ee'}$ and $\tilde{\sigma}_{hh'}$ are given by $\tilde{\sigma}_{ii'} = 4\pi^2\alpha\mathcal{F}^2/(3n_{\text{out}})|\vec{r}_{i,i'}|^2$, where i,i' corresponds to e,e' or h,h' for transitions between (initial and final) electron or hole states, respectively. The fine-structure constant α is here $\sim 1/137$, n_{out} is the refractive index of the medium outside the NC, and $|\vec{r}_{i,i'}|$ is the coordinate matrix element. The (corrective) field factor $\mathcal{F} = 3\varepsilon_{\text{out}}/(\varepsilon_{\text{in}} + 2\varepsilon_{\text{out}})$ accounts for the difference between dielectric constants of the surrounding matrix (ε_{out}) and the NC (ε_{in}). The dielectric constant and refractive index of the SiO_2 matrix are taken as $\varepsilon_{\text{out}} \approx 2$ and $n_{\text{out}} \approx 1.4$, respectively; for the NCs, the bulk static value of the dielectric constant $\varepsilon_{\text{in}} \approx 12$ is used, which yields $\mathcal{F}^2 \approx 0.14$.[18] The coordinate matrix element $|\vec{r}_{i,i'}|$ was calculated including only interatomic matrix elements, which is reasonable for Si.[21] Finally, the normalized Lorentzian function $S_\delta(x)$ with half-width δ is used in Eq. (2) for the energy conservation consideration. For δ, a value of $\delta \approx 10$ meV has been chosen in order to account for the level broadening due to energy relaxation and for the spectral linewidth of the pump pulse.

The IA cross sections found by the tight-binding procedure show a similar spectral dependence for different sizes of NCs [see Fig. 1(a) for exciton energy $\mathcal{E}_{\text{exc}} = 3.5$ eV]. In the investigated NC size range, values of the order of $\sigma_{\text{IA}} \approx 10^{-16}$ cm^2 in the low-photon-energy range are found, followed by a decrease of the absorption cross sections by about one order of magnitude towards higher-photon energies. This dependence can be interpreted to a result from the competition between the growing density of final states and the decrease of the value of the matrix element $|\vec{r}_{i,i'}|$ with the energy difference $E_{i'} - E_i$. For comparison, the theoretical dependence obtained within the Drude model [Eq. (1)] is

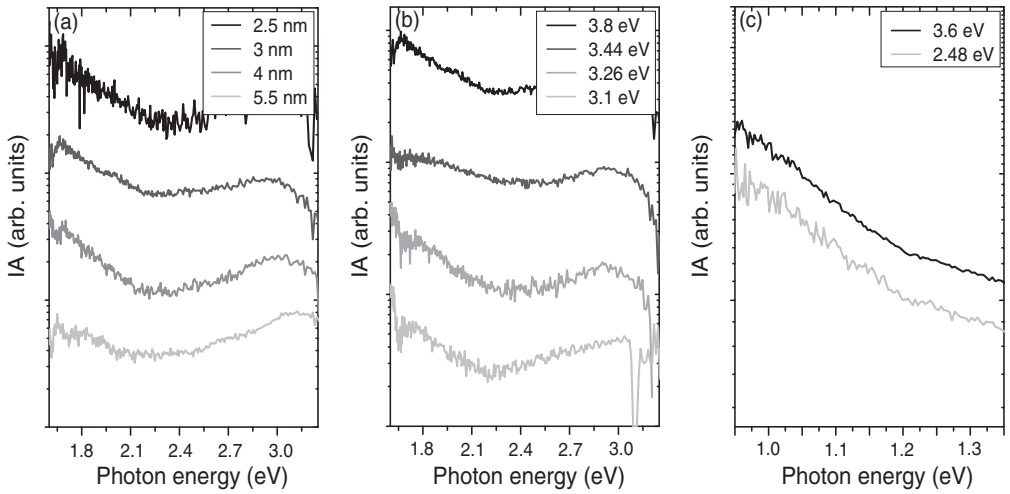

FIG. 2. Experimental spectral dependence of IA. (a) IA spectra in the 1.6–3.25 eV detection range experimentally obtained upon $E_{exc} = 3.8$ eV excitation for the maximum temporal overlap between pump and probe pulse (while avoiding possible initial signal distortions) for samples with different average NC sizes: $d_{NC} = 2.5$, 3, 4, and 5 nm, from black to light gray, respectively. (b) IA spectra in the 1.6–3.25 eV detection range for the sample with average diameter $d_{NC} = 3$ nm under different energy excitation for the maximum temporal overlap between pump and probe pulses. Here, the different traces correspond to excitation at $E_{exc} = 3.8$, 3.44, 3.26, and 3.1 eV (from black to light gray, respectively). (c) IA spectra in the 0.95–1.35 eV detection range for sample with average diameter $d_{NC} = 3$ nm under 3.6 eV (black) and 2.48 eV (light gray) excitation for the maximum temporal overlap between pump and probe pulses. Spectra have been shifted vertically for clarity.

also shown for electrons and holes in bulk Si (light and dark green lines, respectively) and Si NCs (light and dark magenta lines, respectively). Evidently, the results of these calculations show a very similar spectral behavior, slightly diverging from the curves obtained by the tight-binding approach towards higher-photon energies. The amplitude of the IA cross sections for the NC systems is somewhat higher than found for free carriers in bulk Si by the Drude model.

IV. EXPERIMENTAL RESULTS AND COMPARISON WITH THEORETICAL MODEL

In Fig. 2(a), IA spectra (or cross sections) are shown for different average NC sizes obtained for $E_{exc} = 3.8$ eV excitation and probing in the energy range $E_{probe} = 1.6$–3.25 eV for the maximum temporal overlap between pump and probe pulses (while avoiding possible initial signal distortions). The experimental results are vertically shifted for clarity. In agreement with the theoretical tight-binding calculations presented in Fig. 1(a), the results are practically independent of NC size. For all samples, the IA spectra show a gradual decrease in intensity towards higher probe photon energies, followed by a slight increase for the highest energy range [see Fig. 2(a)]. Recently, it has been found that the threshold value marking the onset of that increase shifts towards higher energies for smaller NCs.[11] This was identified with ionization of carriers from an STE state, related to the surface of the NC, into the higher-lying NC core-related levels. Further details on this can be found in Sec. V. Evaluation of the simulated values for the IA cross sections will be discussed later.

The IA spectral dependence on the excitation energy was investigated in the range $E_{exc} = 3.1$–3.8 eV, as shown in Fig. 2(b) for the sample with the average NC diameter of $d_{NC} = 3$ nm for the maximum temporal overlap between pump and probe pulses (spectra are also vertically shifted for clarity). A very similar behavior is observed regardless of the probe photon energy. A similar independence on the excitation energy was also found for the NIR probing range $\{E_{probe} = 0.95$–1.35 eV [see Fig. 2(c)]$\}$. From these results, we conclude that the IA cross section is not influenced by the excitation (and exciton) energy. In order to validate this finding, we have modeled the IA cross sections for NCs with an average size of $d_{NC} = 5$ nm for the exciton energy range $\mathcal{E}_{exc} = 2.0$–4.0 eV and plotted them together with the experimental results [see Fig. 3(a)]. According to the model, the dependence of the IA cross section on $\mathcal{E}_{exc}$ is rather marginal for low-probe photon energies, but diverges in the higher-energy pumping range, with a maximum difference of a factor ~5 between high (4.0 eV) and low (2.0 eV) $\mathcal{E}_{exc}$.

A. IA cross section

In order to directly compare the theoretically obtained values for the IA cross section with the experimental results, the IA cross section has been extracted from the experimental data {for the maximum temporal overlap between pump and probe, thus prior to carrier relaxation [black dashed lines in Fig. 3(a)]}. The values were evaluated using

$$\sigma_{IA} = \alpha_{IA}/(\gamma n_{NC}), \tag{3}$$

where n_{NC} is the NC density (derived from the atomic percentage of excess Si in the sputtered layer and average NC diameter d_{NC}) and α_{IA} the IA coefficient, obtained from the IA data. The parameter γ is the average number of excitons created per NC by the excitation pulse, which for this evaluation is set to $\gamma = 10$, since the measurements were conducted under high-photon flux excitation. Since the real number of excitons per NC is expected to be $N_{exc} \leqslant 10$, the chosen value for γ is strongly overestimated, and therefore the derived values for the IA cross section can be interpreted as a

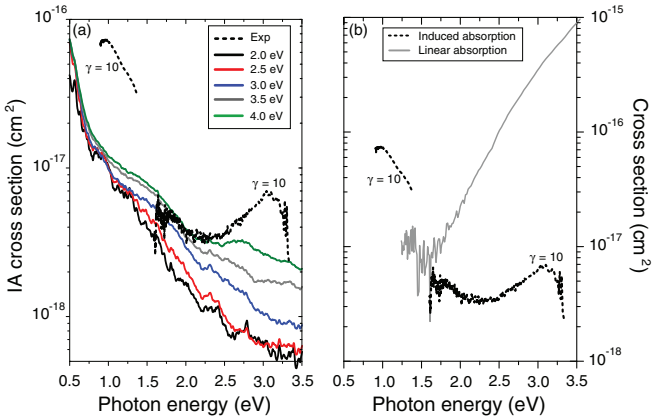

FIG. 3. (Color online) Comparison of experimentally measured IA cross section with theoretical model and with the linear absorption for the sample with average diameter $d_{NC} = 5$ nm. (a) IA cross section obtained from experimental results compared with theoretical modeling for the maximum temporal overlap between pump and probe pulse in the energy range of $E_{probe} = 0.5$–3.5 eV. Different colors correspond to different exciton energies $\mathcal{E}_{exc}$. The black dashed lines are the experimental data obtained under excitation with $E_{exc} = 3.6$ eV scaled down by setting the average number of excitons created per NC to $\gamma = 10$ (see text for further explanation). It should be noted that the signal-to-noise ratios of the IA signal on the edges of the visible and NIR probe pulses are low. (b) Spectral dependence of IA cross section in the visible and NIR plotted together with the linear absorption cross section.

lower limit. With this in mind, we can conclude that the values for σ_{IA} for probing in the visible energy range extracted from experimental data can be well described by the simulation, but only up to a certain threshold value E_{th}. For detection photon energies above E_{th}, the amplitude of the simulations and observations diverge, with the model predicting a gradual decrease for higher-photon energies, while the opposite is observed in experiments. This observation will be further discussed in Sec. V.

For the NIR probing range, the trend of the IA cross section as found by theoretical modeling is in good agreement with the experimental results (σ_{IA} decreasing with increasing E_{probe}), although the amplitude is considerably higher. Since the excitation conditions (e.g., pump fluence) were similar for both visible and NIR detection ranges and since the theoretical model follows the experimental results in the visible detection range (up to E_{th}), the large amplitude of the experimentally obtained IA cross section in the NIR range is not an experimental artifact. From an experimental perspective, it should be noted that for IA signal registration, the reflection of the probe is expected to change negligibly upon pumping, so that the intensity of the registered signal could be fully attributed to IA of the sample. The discrepancy between the model and the experimental results in the NIR range could be due to the fact that the model relies for a greater part on bulk parameters and does not take into account additional effects, such as multiple-photon absorption by the same carrier, resulting in potential underestimation of the value of the IA cross section.

In order to validate our conclusions, we have evaluated the IA cross section in a separate pump-probe experiment conducted on a different setup under single-wavelength probing ($E_{probe} = 0.95$ eV) and low-pumping-fluence excitation (i.e., multiple-photon absorption could be precluded). For pumping, two different excitation energies have been chosen ($E_{exc} = 2.48$ and 4.66 eV).[22] After scaling, the found IA signal according to Eq. (3) (and scaling γ to unity) is of the order of $\sigma_{IA} = 10^{-17}$–10^{-16} cm^2 (not shown) for both excitation energies. Both experiments thus lead to the same result.

Finally, we compared the experimentally obtained IA spectra for the NCs with an average diameter of $d_{NC} = 5$ nm recorded for an excitation energy $E_{exc} = 3.6$ eV with the linear absorption spectrum [see Fig. 3(b)]. The latter has been measured in the range $E_{det} = 1.25$–3.5 eV using a UV-VIS Lambda 900 spectrometer in combination with an integrating sphere so that scattering effects are accounted for. Subsequently, the linear absorption cross section has been deduced. As expected, the amplitude of the linear cross section is significantly larger than the IA cross section in the visible photon energy range (even when considering the extensive downscaling of the intensity of the IA spectrum with $\gamma = 10$). However, for lower-photon energies, the linear absorption rapidly decreases while for the IA the opposite trend is observed. The decrease for the linear absorption can be explained in terms of the lower probability for absorption of photons with an energy approaching the band gap E_g, as momentum mismatch increases. For lower-photon energies $E_{probe} < E_g$ the single-photon linear absorption cross section is zero (for low E_{probe} the signal-to-noise ratio is very low in this measurement). On the other hand, the probability of nonlinear absorption of photons evidently increases significantly for these low energies. We conclude that for lower-photon energies, $E_{probe} \lesssim 1.75$ eV, the IA cross section is considerably larger than that of linear absorption which could potentially be advantageous for solar cells, as will be discussed in the Conclusions.

B. Time-resolved investigations of IA

The evaluation of the IA cross section by the tight-binding approach does not consider any temporal characteristics on the relaxation of excitons. However, from the calculated IA cross section of carriers for decreasing values of $\mathcal{E}_{exc}$, information about their relaxation to lower states in the conduction or valence band can be obtained; it reflects carrier cooling. Based on this notion and the results shown in Fig. 3(a), one would expect that for low-probe photon energies, the IA signal decays marginally due to relaxation within the respective bands, as can be inferred from the quasi-independence of the IA cross section on $\mathcal{E}_{exc}$. For the high-probe photon energy range, one would expect a stronger decay of the IA intensity since the IA cross section is found to decrease for lower $\mathcal{E}_{exc}$. In order to verify this expectation, the dependence of the IA signal has been investigated as a function of the delay time between pump and probe pulses (with a maximum of ∼3.5 ns). In Figs. 4(a) and 4(b), IA spectra are shown for both detection ranges, NIR [$E_{probe} = 0.95$–1.35 eV, Fig. 4(a)] and visible [$E_{probe} = 1.6$–3.25 eV, Fig. 4(b)] for the sample with an average NC diameter of $d_{NC} = 5$ nm under excitation of $E_{exc} = 3.6$ eV for different delay times between pump and probe (as discussed before, the amplitude of the IA signal for

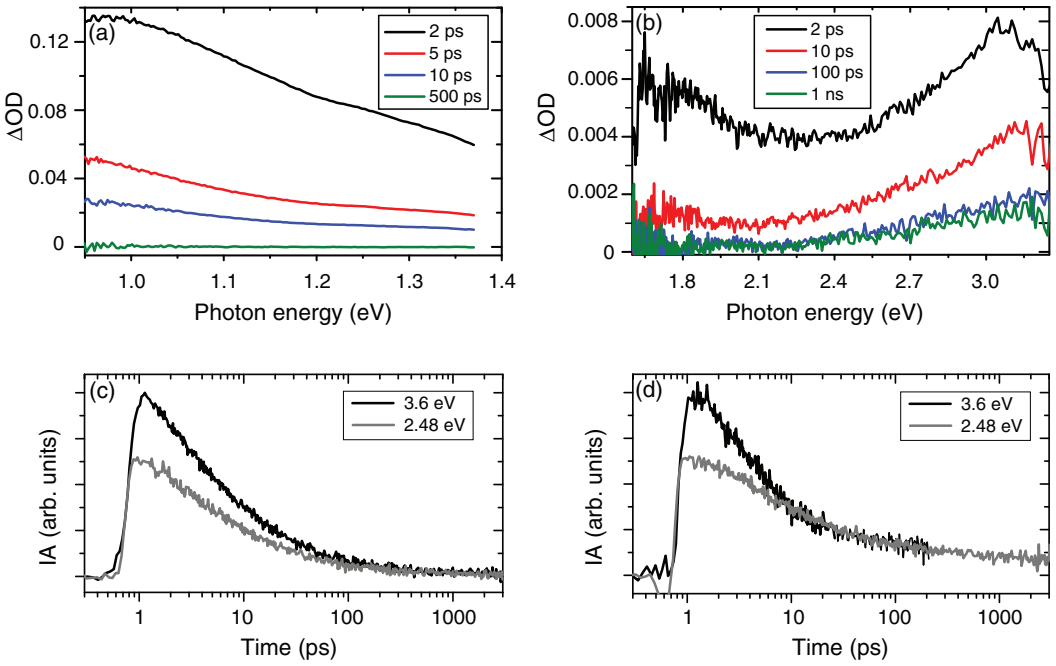

FIG. 4. (Color online) Experimental IA results for sample with an average NC diameter $d_{NC} = 5$ nm under excitation of $E_{exc} = 3.6$ eV. IA spectra in the NIR [panel (a)] and in the visible [panel (b)] ranges for different time delays between pump and probe. IA dynamics recorded at $E_{probe} = 1$ eV [panel (c)] and $E_{probe} = 3$ eV [panel (d)] for two different excitation photon energies of $E_{exc} = 3.6$ eV (black) and $E_{exc} = 2.48$ eV (gray) in a detection time window of ~3.5 ns.

the visible range is about a factor ~10 lower than in NIR.) For low-probe photon energy, the IA signal vanishes within ~500 ps, while for the higher-probe energies exceeding a certain threshold ($E_{th} \approx 2.25$ eV for this sample) the IA signal following the initial ps decay remains even for the maximal delay of 3.5 ns. These features are also visible in the IA dynamics recorded for below- and above-threshold probing ($E_{probe} = 1$ and 3 eV, respectively) which are shown in Figs. 4(c) and 4(d), respectively. In both cases, the dynamics features a fast decay on the 1–100 ps time scale. Since the experiment in this study is conducted under high-photon flux, such that multiple carriers are created per single NC, it is possible that the decay dynamics are initially dominated by Auger recombination of multiple excitons confined in the same NC, which is known to proceed on a subnanosecond time scale.[7,9,22] In both Figs. 4(c) and 4(d), IA dynamics is shown for two excitation energies: $E_{exc} = 3.6$ eV (black) and $E_{exc} = 2.48$ eV (gray). The ratio of ~1.5 between the initial amplitudes of the dynamics for the high- and low-energy excitation can be explained by difference in the number of absorbed photons N_{abs} for these two excitations: $N_{abs}^{3.6\,eV}/N_{abs}^{2.48\,eV} \approx 1.5$. From the similarities in the IA dynamics in the different panels, we conclude that not only the spectral but also the temporal characteristics of IA are fairly independent of excitation (or exciton) energy, with initial fast decaying components and a long (ns–μs) component for above-threshold probe energies. As previously mentioned, in case of probing with high-photon energies [Fig. 4(d)], the (temporal) decay of IA intensity could be (partially) explained in terms of a decreasing IA cross section for lower $\mathcal{E}_{exc}$. Following the theoretical simulations [Fig. 3(a)], the decrease in IA cross section could give rise to a reduction of the IA amplitude by a factor of ~3.5 (between the lowest and highest modeled E_{exc}) for probe photon energy of $E_{probe} = 3$ eV. On the other hand, the "full" relaxation of the IA signal in the low-probe photon energy range [Fig. 4(a)], suggesting complete depletion of carriers, can not be related to this effect, as the IA cross section is found to be approximately constant for $E_{probe} = 1$ eV. Evidently, the model does not include other possible relaxation mechanisms such as trapping, Auger recombination, and other fast (nonradiative) processes, which will also lead to reduction of the IA signal. One or more of these effects should then be responsible for the behavior of the IA signal observed for probe energies below the threshold value E_{th}. As previously mentioned, this behavior can be explained in terms of formation of an STE; details will be discussed in the next section. It should be noted that the apparent "zero" level of the IA dynamics recorded in the NIR range is a result of the limited signal-to-noise ratio for long delay times between pump and probe. This is concluded from previous IA experiments conducted on the same samples with similar excitation photon energies, but orders-of-magnitude lower-photon fluence (so that $N_{abs} \ll 1$).[22,23] Here, the intensity of the (monocolor NIR probing) IA signal for delay times $\Delta t > 500$ ps did not fully decay, giving evidence for the presence of (a small concentration of) free carriers even at longer delay times.

V. FORMATION OF SELF-TRAPPED EXCITON IN SI NCS

For oxygen-terminated Si NCs with diameters $d_{NC} \lesssim 2.5$ nm, the blue-shift in the PL spectrum is not observed, with the PL energy stabilizing in the visible range. This has been explained in terms of the formation of oxygen-related defects at the surface of NCs with

levels appearing in the band gap and participating in the recombination of carriers.[2] Specific microscopic details of these defects are not known, but oxygen is well known to form electrically active defects in bulk Si.[24,25] Among other possibilities, the formation of an STE has been proposed.[26] Support for the existence of the STE state facilitating photon emission in small oxygen-terminated Si NCs was inferred only indirectly from steady-state PL experiments, predominantly from the aforementioned stabilization of the quantum confinement-induced blue-shift of PL and also from the temperature dependence of PL intensity and lifetime.[27] Experimental evidence directly confirming the formation of the STE has been provided only recently from IA studies.[11] This investigation of the STE state was focused on IA detected in the visible range, where the experimental results deviate from the theoretical models, with the measured IA spectrum increasing with probe photon energy for energies exceeding the threshold value $\{E_{\rm th} \approx 2.25$ eV for the sample with an average NC diameter of $d_{\rm NC} = 5$ nm [see Fig. 3(a)]$\}$. The temporal characteristics for probe energies below and above $E_{\rm th}$ [see Figs. 4(c) and 4(d), respectively] are different, as discussed in the previous section, where a long-standing absorption was observed for probe energies in the above-$E_{\rm th}$ range. On the other hand, the observed PL characteristics followed the NC-size-dependent trend as expected from theoretical modeling. Previously, these features have been ascribed to ionization of excitons from a self-trapped state into NC core-related levels, which implied a metastable nature of the self-trapped state.[11] Here, we discuss this in more detail.

In Fig. 5, the scheme for the adiabatic potentials illustrating the STE system is shown. It contains an exciton-plus-surface-local-vibration with a fixed frequency ω_0. The adiabatic potential $U_0(Q)$ corresponds to the absence of an exciton (with Q being the configuration coordinate, where "0" defines the equilibrium position of the vibration), and $U_1(Q)$ to the exciton in the ground state in the NC, the energy difference between the two parabolas is the NC optical band gap $E_{\rm gap}$. The dotted parabola $U_{\rm exc}(Q)$ corresponds to the "hot" exciton created by (optical) excitation with energy $E_{\rm exc} = 3.6$ eV as used in the experiments. Last, the parabola $U(Q - Q_0)$ describes the STE state, where the shift with respect to Q_0 appears due to the strong interaction with a local vibration.[4,15] The parameter $E_{\rm th}$ is the threshold energy for optical excitation, which increases for smaller NC sizes (under the assumption that the energy position of the STE adiabatic potential is independent of NC diameter). The parameter ΔE is defined by the energy difference between the STE ground state and the NC band gap, $\Delta E = E_{\rm STE} - E_{\rm gap}$, and can be considered as the thermal excitation energy from the exciton ground state into the STE. Accordingly, the parameter $\Delta\varepsilon = \Delta E + E_{\rm th}$ defines the energy of the exciton-phonon coupling, and should remain constant for all NC sizes according experimental results presented in Ref. 11. The Huang-Rhys factor is given by expression[28]

$$S_{\rm HR} = \frac{\Delta\varepsilon}{\hbar\omega_0} = \frac{\Delta E + E_{\rm th}}{\hbar\omega_0}, \tag{4}$$

with fixed phonon frequency ω_0; the plus sign in the equation follows from the metastable nature of the STE state.

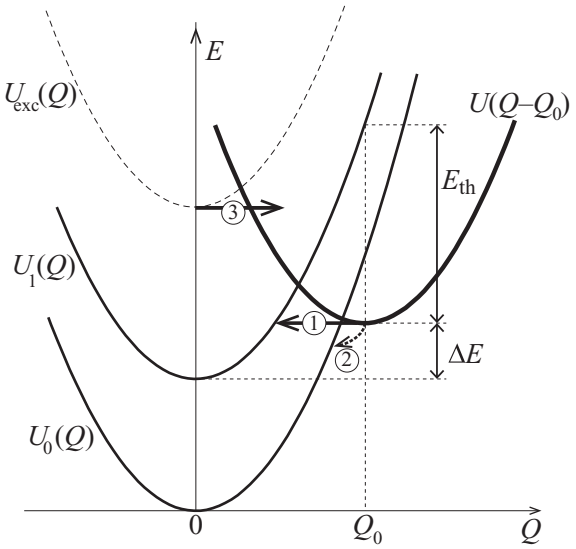

FIG. 5. Configuration coordinate diagram with adiabatic potentials for ground $[U_0(Q)]$, free exciton $[U_1(Q)]$, and STE $[U(Q - Q_0)]$ states. The minimum of the parabola for the STE is shifted to Q_0 compared to the free-exciton adiabatic potential. The dotted parabola $U_{\rm exc}(Q)$ corresponds to a "hot" exciton created by optical excitation. The hot exciton can be captured at the STE state (process "3") and relax to the ground STE state by emitting local phonons. The trapped exciton can return to the free-exciton state by thermally stimulated tunneling (process "1") or optical reexcitation if the energy is larger than threshold energy $E_{\rm th}$. It can also recombine nonradiatively into $U_0(Q)$ (process "2"). ΔE corresponds to the energy difference between the bottom of the free exciton and the STE adiabatic potential.

In the proposed model, the STE lifetime $\tau_{\rm l}^{\rm STE}$ should be determined by thermally stimulated tunneling ionization (process "1" in Fig. 5) and nonradiative recombination from the STE state (process "2" in Fig. 5) with probabilities $W_{\rm t}$ and $W_{\rm NR}$, respectively. In Ref. 29, it has been shown that the radiative recombination rate of the STE is negligible compared to the nonradiative multiphonon recombination rate. For the STE lifetime $\tau_{\rm l}^{\rm STE}$ we therefore arrive at

$$\left(\tau_{\rm l}^{\rm STE}\right)^{-1} = W_{\rm t} + W_{\rm NR}. \tag{5}$$

The probability of nonradiative recombination of the STE $W_{\rm NR}$ is estimated to be about 10^6 s^{-1} in Ref. 29 and comparable with the probability of thermally stimulated tunneling ionization $W_{\rm t}$ for the smallest NCs. In the proposed model, the decay dynamics for the above-threshold probing reflects the STE lifetime and corresponds to its slow component [see the transients in Fig. 4(d)].

The probability of thermally stimulated tunneling ionization $W_{\rm t}$ is determined by the equation

$$W_{\rm t} \equiv \tau_{\rm t}^{-1} = w_{\rm e} J(S_{\rm HR}, T, p), \tag{6}$$

where $w_{\rm e}$ is the pure electron transition probability and $J(S_{\rm HR}, T, p)$ is the overlap integral of oscillator wave functions which depends on temperature T, and the parameter $p = \Delta E/\hbar\omega_0$, which is the number of phonons involved in the transition. The expression for the overlap integral is

given by

$$J(S_{\mathrm{HR}}, T, p) = I_p\left(\frac{S_{\mathrm{HR}}}{\sinh(\theta)}\right) e^{-\left(\frac{S_{\mathrm{HR}}}{\tanh(\theta)} + p\theta\right)}, \tag{7}$$

where $I_p(x)$ is the Bessel function of an imaginary argument and $\theta = \hbar\omega_0/2kT$.[28] Under the assumption that w_e is independent of the vibration coordinate, it can be treated as a parameter. The thermally stimulated tunneling ionization probability W_t is connected to the capture probability W_c of the free exciton at the STE state. For the probability of the capturing process, we can use Eq. (6), where the parameter p is now given by $(E_{\mathrm{exc}} - E_{\mathrm{STE}})/\hbar\omega_0$. We remark that in this approximation the capture probability only depends on E_{exc} and that it is independent of the NC size. The capture probability W_c can be extracted from the initial fast component of the IA dynamics for low-probe energies [see Fig. 4(c)]. From this we conclude that W_c should be in the range 10^{10}–10^{12} s^{-1} (also in agreement with Ref. 10).

The parameter ΔE can not be extracted from experiments. However, following the notion that the position of the PL spectrum stabilizes for NC sizes below $d_{\mathrm{NC}} \lesssim 2.5$ nm, we conclude that for the smallest investigated NCs ($d_{\mathrm{NC}} = 2.5$ nm) ΔE should be small. In Ref. 11, the energy of the electron-phonon coupling $\Delta\varepsilon = 2.75$ eV has been used for calculation of W_t for all the investigated NC sizes. Using this value together with the experimentally obtained optical threshold energy $E_{\mathrm{th}} \approx 2.75$ eV for $d_{\mathrm{NC}} \approx 2.5$ nm gives $\Delta E \approx 0$. Correspondingly, the energy of the STE state should be $E_{\mathrm{STE}} \approx 1.8$ eV.

The second parameter, the phonon energy $\hbar\omega_0$, is estimated to be in the range $\hbar\omega_0 \approx 130$–$170$ meV following observations for similar oxygen-passivated Si NCs by means of single NC spectroscopy.[30] In Ref. 11, a value of 140 meV is used resulting in a Huang and Rhys factor of $S_{\mathrm{HR}} \approx 20.1$. A slightly larger value for $\Delta E \approx 0.15$ eV (and therefore $E_{\mathrm{STE}} = 1.93$ eV) has been used in Ref. 29, resulting in Huang-Rhys factors of $S_{\mathrm{HR}} \approx 20.4$ and $S_{\mathrm{HR}} \approx 19.0$ for $\hbar\omega_0 = 140$ and 150 meV, respectively. The calculated values for the tunneling probability W_t for various sizes of NCs and two temperatures (300 and 77 K) are presented in Ref. 29.

It has been found that the tunneling probability W_t is only slightly dependent on the considered values of the parameters $\hbar\omega_0$ and $\Delta E/E_{\mathrm{STE}}$, and that they are of the order of 10^8 s^{-1} for the larger NCs ($d_{\mathrm{NC}} = 4$–5 nm), but decreases considerably for $d_{\mathrm{NC}} \lesssim 2.5$ nm. For the larger NCs, W_t is much larger than the nonradiative recombination probability W_{NR}, indicating that most trapped excitons return to the free exciton states. However, for smaller NCs, W_t becomes comparable to W_{NR}, suggesting that the PL efficiency decreases. In addition, it has been found that the tunneling probability W_t decreases with lowering temperature. Consequently, we have attempted to confirm the proposed model by investigating the temperature dependence of PL lifetime and intensity. We have experimentally found that the PL lifetime increased significantly from tens of μs at 293 K to several ms for 4.2 K. Similar results for exciton emission from Si NCs have been reported before (e.g., Refs. 12, 27, and 31) and were explained as arising due to singlet-triplet splitting[32] of the exciton ground state. However, as pointed out by, among others, Zhuravlev *et al.*,[27] similar splitting could also appear in the STE state. We therefore conclude that the investigations of temperature-induced changes of PL are not capable of delivering specific fingerprints of the tunneling process invoked in the discussed relaxation mechanism.

VI. CONCLUSIONS

We have performed transient absorption experiments on Si NCs with different average diameters embedded in an SiO_2 matrix in a broad spectral detection range ($E_{\mathrm{probe}} = 0.95$–$1.35$ and 1.6–3.25 eV) for a maximum time window of $\sim$3.5 ns. For the maximum temporal overlap between pump and probe pulse, the IA spectrum in the low-photon-energy range was found to be about one order of magnitude higher in intensity than for high-photon energies (in the visible range), practically following the dependence as predicted by the Drude model. From the amplitude of the IA signal, the IA cross section was inferred, which was successfully modeled using an empirical $sp^3d^5s^*$ tight-binding technique. The experimentally obtained trend could be well described for probe photon energies up to a certain threshold, although the values in the NIR range were modeled to be about one order of magnitude lower (i.e., $\sigma_{\mathrm{IA}} \approx 10^{-16}$–$10^{-17}$ cm^2) than the ones extracted from measurements. On the higher-probe energy side of the spectrum (for above-threshold photon energies), a mismatch between theory and experiments was explained by formation of an STE arising due to surface-related states. Within the STE scenario (described by the Huang-Rhys model), the observed NC-size-dependent spectral threshold behavior as well as temporal characteristics of IA found for below- and above-threshold probing could be well described. For the latter, the IA signal for all probe photon energies featured a decay component of $\tau_{\mathrm{IA}} = 10^{-12}$–$10^{-10}$ s. An additional ns–μs component (i.e., outside of the determination window) was found only for above-threshold photon energies. The initial fast component was assigned to Auger recombination of multiple carriers in the same NC and efficient trapping of carriers (i.e., the formation of the STE), while the slower one was attributed to the ionization of carriers from the STE state back into NC core-related levels. As shown by simulations, formation of an STE does not influence emission for large Si NCs for which the STE energy exceeds the band gap, and the thermally activated release is efficient ($W_t \approx 10^8$ s^{-1}). The situation changes for small NCs, with the STE state dominating the PL mechanism ($W_t \approx 10^5$–10^6 s^{-1}).

Finally, the IA and the linear absorption cross sections σ_{IA} and $\sigma_{\mathrm{lin\ abs}}$ were compared. In the NIR range, σ_{IA} was found to be at least one order of magnitude higher than $\sigma_{\mathrm{lin\ abs}}$, whereas for the higher-photon-energy range it was significantly lower. This feature of Si NCs could potentially be interesting for solar-cell applications since it would allow the low-energy photons, which are generally lost in (the linear) absorption process, to be absorbed by free carriers promoting them to higher-energy states: "hot" carriers. Since the probability of the band-to-band absorption of higher-energy photons is orders of magnitude larger than the absorption by free carriers, the most likely process to occur is the creation of free carriers by visible photons and the subsequent increase of their energy by IA of low-energy ones. The generated hot carriers could potentially be captured and/or extracted as is being done in the configuration of a so-called "hot-carrier cell." For

excitons with energy exceeding twice the band gap, multiple carriers might be created, after which they could separate into adjacent NCs.[22,23,33–35] Alternatively, they could undergo radiative recombination and convert the sequentially absorbed photons into a band for which a higher conversion efficiency could be realized (spectral conversion).[36]

ACKNOWLEDGMENTS

The authors acknowledge M. Fujii (Kobe University) for sharing expertise on the preparation of sputtered layers. This work has been financially supported by Stichting voor de Technologische Wetenschappen (STW).

*E. M. L. D.deJong@uva.nl

[1] D. Kovalev, H. Heckler, G. Polisski, and F. Koch, Phys. Status Solidi **215**, 871 (1999).

[2] M. V. Wolkin, J. Jorne, P. M. Fauchet, G. Allan, and C. Delerue, Phys. Rev. Lett. **82**, 197 (1999).

[3] F. Trojánek, K. Neudert, P. Malý, K. Dohnalová, and I. Pelant, J. Appl. Phys. **99**, 116108 (2006).

[4] A. N. Poddubny and S. V. Goupalov, Phys. Rev. B **77**, 075315 (2008).

[5] A. S. Moskalenko, J. Berakdar, A. N. Poddubny, A. A. Prokofiev, I. N. Yassievich, and S. V. Goupalov, Phys. Rev. B **85**, 085432 (2012).

[6] V. I. Klimov, C. J. Schwarz, D. W. McBranch, and C. W. White, Appl. Phys. Lett. **73**, 2603 (1998).

[7] M. C. Beard, K. P. Knutsen, P. Yu, J. M. Luther, Q. Song, W. K. Metzger, R. J. Ellingson, and A. J. Nozik, Nano Lett. **7**, 2506 (2007).

[8] W. de Boer, H. Zhang, and T. Gregorkiewicz, Mater. Sci. Eng.: B **159**, 190 (2009).

[9] F. Trojánek, K. Neudert, M. Bittner, and P. Malý, Phys. Rev. B **72**, 075365 (2005).

[10] W. D. A. M. de Boer, D. Timmerman, K. Dohnalová, I. N. Yassievich, H. Zhang, W. J. Buma, and T. Gregorkiewicz, Nat. Nanotechnol. **5**, 878 (2010).

[11] W. D. A. M. de Boer, D. Timmerman, T. Gregorkiewicz, H. Zhang, W. J. Buma, A. N. Poddubny, A. A. Prokofiev, and I. N. Yassievich, Phys. Rev. B **85**, 161409(R) (2012).

[12] S. Takeoka, M. Fujii, and S. Hayashi, Phys. Rev. B **62**, 16820 (2000).

[13] R. A. Smith, *Semiconductors*, 1st ed. (Cambridge University Press, New York, 1959).

[14] R. D. Kekatpure and M. L. Brongersma, Nano Lett. **8**, 3787 (2008).

[15] V. N. Abakumov, V. I. Perel, and I. N. Yassievich, *Nonradiative Recombination in Semiconductors* (North-Holland, Amsterdam, 1991).

[16] C. Bulutay, Phys. Rev. B **76**, 205321 (2007).

[17] J.-M. Jancu, R. Scholz, F. Beltram, and F. Bassani, Phys. Rev. B **57**, 6493 (1998).

[18] C. Delerue and M. Lannoo, *Nanostructures: Theory and Modelling* (Springer, Berlin, 2004).

[19] N. A. Hill and K. B. Whaley, J. Electron. Mater. **25**, 269 (1996).

[20] A. N. Poddubny, A. A. Prokofiev, and I. N. Yassievich, Appl. Phys. Lett. **97**, 231116 (2010).

[21] M. Cruz, M. R. Beltrán, C. Wang, J. Tagüeña-Martínez, and Y. G. Rubo, Phys. Rev. B **59**, 15381 (1999).

[22] W. D. A. M. de Boer, M. T. Trinh, D. Timmerman, J. M. Schins, L. D. A. Siebbeles, and T. Gregorkiewicz, Appl. Phys. Lett. **99**, 053126 (2011).

[23] M. T. Trinh, R. Limpens, W. D. A. M. de Boer, J. M. Schins, L. D. A. Siebbeles, and T. Gregorkiewicz, Nat. Photonics **6**, 316 (2012).

[24] H. H. P. Th. Bekman, T. Gregorkiewicz, D. A. van Wezep, and C. A. J. Ammerlaan, J. Appl. Phys. **62**, 4404 (1987).

[25] T. Gregorkiewicz, D. A. van Wezep, H. H. P. Th. Bekman, and C. A. J. Ammerlaan, Phys. Rev. Lett. **59**, 1702 (1987).

[26] G. Allan, C. Delerue, and M. Lannoo, Phys. Rev. Lett. **76**, 2961 (1996).

[27] K. S. Zhuravlev and A. Yu. Kobitsky, Semiconductors **34**, 1203 (2000).

[28] K. Huang and A. Rhys, Proc. R. Soc. London, Ser. A **204**, 406 (1950).

[29] A. V. Gert and I. N. Yassievich, JETP Lett. **97**, 87 (2013).

[30] H. J. Hrostowski and R. H. Kaiser, Phys. Rev. **107**, 966 (1957).

[31] A. Yu. Kobitski, K. S. Zhuravlev, H. P. Wagner, and D. R. T. Zahn, Phys. Rev. B **63**, 115423 (2001).

[32] P. D. J. Calcott, K. J. Nash, L. T. Canham, M. J. Kane, and D. Brumhead, J. Phys.: Condens. Matter **5**, L91 (1993).

[33] D. Timmerman, J. Valenta, K. Dohnalová, W. D. A. M. de Boer, and T. Gregorkiewicz, Nat. Nanotechnol. **6**, 710 (2011).

[34] D. Timmerman, I. Izeddin, P. Stallinga, I. N. Yassievich, and T. Gregorkiewicz, Nat. Photonics **2**, 105 (2008).

[35] M. Govoni, I. Marri, and S. Ossicini, Nat. Photonics **6**, 672 (2012).

[36] W. de Boer and T. Gregorkiewicz, SPIE Newsroom, http://spie.org/x85681.xml (March 2012).